

Nearly invariant boundary entanglement in optomechanical systems

Shi-Wei Cui(崔世威), Zhi-Jiao Deng(邓志姣), Chun-Wang Wu(吴春旺), and Qing-Xia Meng(孟庆霞)
Citation: Chin. Phys. B, 2021, 30 (**11**): 110311. DOI: 10.1088/1674-1056/ac16ca
Journal homepage: http://cpb.iphy.ac.cn; http://iopscience.iop.org/cpb

What follows is a list of articles you may be interested in

Tunable ponderomotive squeezing in an optomechanical system with two coupled resonators

Qin Wu(吴琴)
Chin. Phys. B, 2021, 30 (**2**): 020303. DOI: 10.1088/1674-1056/abb7f5

Generating Kerr nonlinearity with an engineered non-Markovian environment

Fei-Lei Xiong(熊飞雷), Wan-Li Yang(杨万里), Mang Feng(冯芒)
Chin. Phys. B, 2020, 29 (**4**): 040302. DOI: 10.1088/1674-1056/ab7741

Quantifying non-classical correlations under thermal effects in a double cavity optomechanical system

Mohamed Amazioug, Larbi Jebli, Mostafa Nassik, Nabil Habiballah
Chin. Phys. B, 2020, 29 (**2**): 020304. DOI: 10.1088/1674-1056/ab65b6

Optomechanical state transfer between two distant membranes in the presence of non-Markovian environments

Jiong Cheng(程泂), Xian-Ting Liang(梁先庭), Wen-Zhao Zhang(张闻钊), Xiangmei Duan(段香梅)
Chin. Phys. B, 2018, 27 (**12**): 120302. DOI: 10.1088/1674-1056/27/12/120302

Controlling the entanglement of mechanical oscillators in composite optomechanical system

Jun Zhang(张俊), Qing-Xia Mu(穆青霞), Wen-Zhao Zhang(张闻钊)
Chin. Phys. B, 2018, 27 (**4**): 040304. DOI: 10.1088/1674-1056/27/4/040304

Nearly invariant boundary entanglement in optomechanical systems*

Shi-Wei Cui(崔世威)[1,2], Zhi-Jiao Deng(邓志姣)[1,2,†], Chun-Wang Wu(吴春旺)[1,2], and Qing-Xia Meng(孟庆霞)[3]

[1] *Department of Physics, College of Liberal Arts and Sciences, National University of Defense Technology, Changsha* 410073, *China*
[2] *Interdisciplinary Center for Quantum Information, National University of Defense Technology, Changsha* 410073, *China*
[3] *Northwest Institute of Nuclear Technology, Xi'an* 710024, *China*

(Received 19 June 2021; revised manuscript received 17 July 2021; accepted manuscript online 22 July 2021)

In order to understand our previous numerical finding that steady-state entanglement along the instability boundary remains unchanged in a three-mode optomechanical system [*Phys. Rev. A* **101** 023838 (2020)], we investigate in detail the boundary entanglement in a simpler two-mode optomechanical system. Studies show that both the mechanism to generate entanglement and the parameter dependence of boundary entanglement are quite similar in these two models. Therefore, the two-mode system has captured the main features in the three-mode system. With the help of analytical calculations and discussing in a much bigger parameter interval, we find that the unchanging behavior previously discovered is actually an extremely slow changing behavior of the boundary entanglement function, and most importantly, this nearly invariant boundary entanglement is a general phenomenon via parametric down conversion process in the weak dissipation regime. This is by itself interesting as threshold quantum signatures in optomechanical phonon lasers, or may have potential value in related applications based on boundary quantum properties.

Keywords: boundary entanglement, optomechanical system

PACS: 03.65.Ud, 42.65.Sf, 42.50.Wk **DOI:** 10.1088/1674-1056/ac16ca

1. Introduction

Optomechanics,[1,2] which deals with nonlinear interaction between photons and phonons, has attracted a lot of attentions due to its potential applications in fundamental studies of quantum mechanics, precise measurement and quantum information processing. The single-photon optomechanical coupling is experimentally quite weak,[3,4] so a cavity with driving laser is needed to amplify the interaction effects.[5] With appropriate driving laser detuning, both cooling and heating of mechanical motions are reachable.[6] To raise the heating rate by increasing the driving power, the system goes to instability once the overall mechanical damping rate becomes negative.[7]

The transition from stability to instability might accompanying interesting quantum features in the vicinity of their boundary, for example, driving the system near the instability boundary can enhance the nonlinearity at single-photon level,[8] or increase the steady-state entanglement,[9] or exhibit divergent as well as negative susceptibilities, which is beneficial to quantum sensing.[10] Based on a three-mode optomechanical system, we even recently discover that the steady-state entanglement along the boundary line remains unchanged, and it is very robust to thermal phonon noise, thus providing a strong quantum signature of transitions from stable fixed points to limit cycles.[11,12] However, due to the calculation complexity, we can only resort to numerical integrations and the parameter space involved is very limited. Therefore, several questions arise: Does this phenomenon of invariant boundary entanglement depend on the specific model? Can we learn more from simpler models?

In this article, we will investigate the boundary entanglement in the simplest two-mode optomechanical system, where one optical mode is coupled with mechanical vibration by radiation pressure force.[13] With the help of some analytical calculation and discussing in a much bigger parameter interval, we find that the invariant boundary entanglement is by no means completely invariant, but the change is so small that it can be regarded as unchanged, and this nearly invariant boundary entanglement is a general phenomenon via parametric down conversion process in the weakly dissipative region, *i.e.*, the vibration has a very high mechanical quality factor Q, larger than the order of $O(10^3)$. This happens to be the region discussed in our previous three-mode system.[11,12] Most state-of-the-art experiments can reach the resolved sideband regime and the quality factor can range from 10^4 to 10^9.[1] The nonlinear phenomena can be enhanced in this region with smaller mechanical damping rate $\gamma_{\rm m} = \omega_{\rm m}/Q$, since it needs less driving power to get instability. Besides, the nonlinear dynamics with red laser detuning also show sensitivity to initial conditions.[14] Here, we focus on the blue laser detuning to generate photon-phonon entanglement through typical parametric down conversion $\propto {\rm e}^{-{\rm i}\omega_{\rm L}t}\hat{a}^{\dagger}\hat{b}^{\dagger}$, where $\omega_{\rm L}$ is the pumping laser frequency, $\hat{a}^{\dagger}$ and $\hat{b}^{\dagger}$ are creation operators of optical and mechanical modes with frequencies $\omega_{\rm a}$ and $\omega_{\rm m}$, respectively. The value of boundary entanglement remains almost unchanged in a wide driving detuning interval around the res-

*Project supported by the National Natural Science Foundation of China (Grant Nos. 11574398, 11904402, 12074433, and 12004430) and the National Basic Research Program of China (Grant No. 2016YFA0301903).

†Corresponding author. E-mail: dengzhijiao926@hotmail.com

© 2021 Chinese Physical Society and IOP Publishing Ltd

onant driving $\omega_{\rm L}=\omega_{\rm a}+\omega_{\rm m}$, and equals approximately twice the ratio of intrinsical mechanical and optical damping rates when this ratio is much smaller than one. Since both the mechanism to generate entanglement and the parameter dependence of boundary entanglement are quite similar as in our three-mode system, we believe that the two-mode system has captured the main features in the three-mode system. The studies in this paper can not only complement our former study on boundary entanglement,[11,12] but also extend to a more general conclusion that parametric down conversion plus weak mechanical dissipation can lead to nearly invariant boundary entanglement.

Our paper is organized as follows: in Section 2, we will review the two-mode optomechanical system and show our finding of nearly invariant boundary entanglement in this system. In Section 3, with some analytical calculation, we analyze how the boundary entanglement at resonant driving depends on the system parameters, and then compare the boundary entanglement in the weak and strong dissipation regions. In Section 4, we study and discuss how the boundary entanglement changes with various other parameters in the weak dissipation regime. In all these sections, we will mention the three-mode situations in appropriate places for comparison. In Section 5, we summarize our results.

2. Physical system and boundary entanglement

The two-mode optomechanical system, which contains the main characteristics of photon-phonon interaction, has been well studied in many aspects.[1] A typical experimental setup is a driven Fabry–Perot cavity with one mirror fixed and the other free to vibrate.[5] The Hamiltonian of the whole system is[13,15]

$$\begin{aligned}\hat{H}=&\hbar\omega_{\rm a}\hat{a}^{\dagger}\hat{a}-\hbar g_0\hat{a}^{\dagger}\hat{a}\hat{q}+\frac{\hbar\omega_{\rm m}}{2}(\hat{p}^2+\hat{q}^2)\\&+{\rm i}\hbar\Lambda(\hat{a}^{\dagger}{\rm e}^{-{\rm i}\omega_{\rm L}t}-\hat{a}{\rm e}^{{\rm i}\omega_{\rm L}t}),\end{aligned}\tag{1}$$

where the optical cavity mode with frequency $\omega_{\rm a}$ is coupled with the mechanical vibration by a strength g_0. The operators $\hat{q}=(\hat{b}^{\dagger}+\hat{b})/\sqrt{2}$, $\hat{p}=(\hat{b}-\hat{b}^{\dagger})/(\sqrt{2}{\rm i})$ represent the dimensionless position and momentum of the mechanical mode having frequency $\omega_{\rm m}$, respectively. The last term denotes the driving of cavity mode by a laser with amplitude Λ and frequency $\omega_{\rm L}$.

The dissipative dynamics of the system is described by the quantum Langevin equations (written in the interaction picture with respect to $\hbar\omega_{\rm L}\hat{a}^{\dagger}\hat{a}$),[16]

$$\begin{aligned}\dot{\hat{a}}&=\left({\rm i}\Delta-\frac{\kappa}{2}\right)\hat{a}+{\rm i}g_0\hat{a}\hat{q}+\Lambda+\sqrt{\kappa}\hat{a}_{\rm in},\\\dot{\hat{q}}&=\omega_{\rm m}\hat{p},\\\dot{\hat{p}}&=-\omega_{\rm m}\hat{q}+g_0\hat{a}^{\dagger}\hat{a}-\gamma_{\rm m}\hat{p}+\hat{\xi}.\end{aligned}\tag{2}$$

Here $\Delta=\omega_{\rm L}-\omega_{\rm a}$ describes the driving laser detuning from the cavity resonance,[17] $\gamma_{\rm m}$ is the mechanical damping rate, and κ is the cavity intensity decay rate. The vacuum radiation input noise $\hat{a}_{\rm in}$ with zero mean, has only one nonzero correlation function $\langle\hat{a}_{\rm in}(t)\hat{a}_{\rm in}^{\dagger}(t')\rangle=\delta(t-t')$. The Hermitian Brownian noise operator $\hat{\xi}$, whose average value is also zero, satisfies

$$\langle\hat{\xi}(t)\hat{\xi}(t')+\hat{\xi}(t')\hat{\xi}(t)\rangle/2=\gamma_{\rm m}(2\bar{n}+1)\delta(t-t')$$

when $\omega_{\rm m}\gg\gamma_{\rm m}$,[18] where $\bar{n}=[\exp(\hbar\omega_{\rm m}/(k_{\rm B}T))-1]^{-1}$ is the mean thermal phonon number at temperature T.

In the case of weak coupling $g_0\ll\kappa$ and moderate driving Λ, equation (2) can be solved by the mean-field approximation,[1] *i.e.*, decomposing each operator $\hat{O}$ into its mean value $\langle\hat{O}\rangle\equiv O$ plus the quantum fluctuation $\delta\hat{O}$ around the mean value. By doing this, the equations of motion can be separated into two sets, one describes the classical behavior reflected by mean values, the other provides the quantum fluctuations around the classical orbit. The set of classical mean value equations takes the following form:

$$\begin{aligned}\dot{a}&=({\rm i}\Delta-\kappa/2)a+{\rm i}g_0aq+\Lambda,\\\dot{q}&=\omega_{\rm m}p,\\\dot{p}&=-\omega_{\rm m}q+g_0|a|^2-\gamma_{\rm m}p,\end{aligned}\tag{3}$$

whose nonlinear classical dynamics has been widely studied including bistability,[19] limit cycles,[20] chaos,[21] *etc*. Its fixed points are the solutions by letting all the first-order derivatives to be zeros, *i.e.*,

$$\begin{aligned}&p_{\rm s}=0,\quad q_{\rm s}=(g_0/\omega_{\rm m})|a_{\rm s}|^2,\\&a_{\rm s}=\Lambda[\kappa/2-{\rm i}(\Delta+(g_0^2/\omega_{\rm m})|a_{\rm s}|^2)]^{-1}.\end{aligned}$$

Their stability analysis is related to the linearized equations of motion for quantum fluctuations[16]

$$\dot{\boldsymbol{A}}(t)=\boldsymbol{S}(t)\boldsymbol{A}(t)+\boldsymbol{n}(t),\tag{4}$$

where

$$\begin{aligned}\boldsymbol{A}^{\rm T}(t)&=(\delta\hat{a},\ \delta\hat{a}^{\dagger},\ \delta\hat{q},\ \delta\hat{p}),\\\boldsymbol{n}^{\rm T}(t)&=(\sqrt{\kappa}\hat{a}_{\rm in},\ \sqrt{\kappa}\hat{a}_{\rm in}^{\dagger},\ 0,\ \hat{\xi}(t)),\end{aligned}$$

and the Jacobian matrix $\boldsymbol{S}$ is given by

$$\boldsymbol{S}(t)=\begin{pmatrix}{\rm i}\Delta-\kappa/2+{\rm i}g_0q & 0 & {\rm i}g_0a & 0\\0 & -{\rm i}\Delta-\kappa/2-{\rm i}g_0q & -{\rm i}g_0a^* & 0\\0 & 0 & 0 & \omega_{\rm m}\\g_0a^* & g_0a & -\omega_{\rm m} & -\gamma_{\rm m}\end{pmatrix}.\tag{5}$$

The dynamics of $\boldsymbol{S}(t)$ is determined by Eq. (3), which combined with Eq. (4) can predict the quantum dynamics of the whole system as long as none of the Lyapunov exponents of the classical equations are positive.[22] To judge the stability of one particular fixed point, we evaluate matrix $\boldsymbol{S}$ at that fixed point. It is stable when all of the eigenvalues of $\boldsymbol{S}$ have negative real parts.

The mechanism to generate photon–phonon entanglement is easily to be understood from the linearized Hamiltonian $\hat{H}_{\rm eff} \simeq -\hbar\Delta\delta\hat{a}^{\dagger}\delta\hat{a} + \hbar\omega_{\rm m}(\delta\hat{p}^2+\delta\hat{q}^2)/2 - \hbar g_0(a\delta\hat{a}^{\dagger} + a^{*}\delta\hat{a})\delta\hat{q}$. When the driving detuning $\Delta \simeq \omega_{\rm m}$, *i.e.*, $\omega_{\rm L} \simeq \omega_{\rm a}+\omega_{\rm m}$, the interaction term $\propto g_0(a\delta\hat{a}^{\dagger}\delta\hat{b}^{\dagger} + a^{*}\delta\hat{a}\delta\hat{b})$ plays a major role. This term is a typical parametric down conversion process, with in-coming driving photon with frequency $\omega_{\rm L}$ disappeared, meanwhile a cavity photon with frequency $\omega_{\rm a}$ and a phonon with frequency $\omega_{\rm m}$ are produced. Moreover, this two-mode squeezing interaction term will inevitably give rise to quantum entanglement between the optical and mechanical modes.[16,23,24] Similarly, the parametric down conversion process $\propto \hat{c}_1\hat{c}_2^{\dagger}\hat{b}^{\dagger} + \hat{c}_1^{\dagger}\hat{c}_2\hat{b}$ is also utilized to generate entanglement in the three-mode system.[11,25,26] It involves one mechanical mode (*i.e.*, $\hat{b}$) and two optical supermodes (*i.e.*, $\hat{c}_1$ and $\hat{c}_2$) separated by frequency difference $2J$, where J denotes the tunneling rate of two local optical cavity modes constituting the supermodes. When the resonant condition, *i.e.*, the frequency difference $2J$ equals the mechanical frequency $\omega_{\rm m}$, is satisfied, driving the higher frequency supermode (*i.e.*, $\hat{c}_1$) with variable laser amplitude and frequency yields the phenomenon of invariant boundary entanglement.[12]

To discuss the boundary entanglement in the two-mode system, we first plot the stability diagram as a function of the driving amplitude and driving detuning in Fig. 1(a). The blue detuning ($\Delta > 0$) region is chosen, where the resonant driving $\Delta = \omega_{\rm m}$ is included and each set of parameters has only one fixed point solution. The boundary line can be solved analytically from the eigenvalues of $\boldsymbol{S}$ matrix, but the expression is too cumbersome to be presented here. The black boundary line obtained from the analytical expression is completely consistent with the numerical results. It has a single peak pointing to the left at the resonant driving, where the interaction is most efficient thus the instability occurs at the lowest driving power.

Due to numerical discreteness, the points can never be located exactly on the boundary. When approaching the boundary from the stable region, the closer the point is to the boundary, the much longer it takes to converge to the fixed point. Correspondingly, quantum entanglement will converge to a stable value in a long-time limit. The steady-state quantum entanglement between optical and mechanical modes is calculated by using logarithmic negativity,[27] which after the linearization treatment is fully determined by the covariance matrix $V(\infty)$, with its elements given by $V_{ij} = (\langle u_i(t)u_j(t) + u_j(t)u_i(t)\rangle)/2$, and $u^{\rm T} = ((\delta\hat{a}+\delta\hat{a}^{\dagger})/\sqrt{2}, (\delta\hat{a}-\delta\hat{a}^{\dagger})/(\sqrt{2}{\rm i}), \delta\hat{q}, \delta\hat{p})$.[28] The logarithmic negativity is defined as $E_N = \max[0, -\ln 2\eta^{-}]$, where η^{-} is the smaller symplectic eigenvalue of the partial transpose of matrix $V(\infty)$.[16] As pointed out in Ref. [11], quantum fluctuations have a tendency to diverge in a tiny range close to the boundary, which makes the linearization method inapplicable. Therefore, this tiny range is excluded in the calculation, but the selected boundary points are close enough to indicate the boundary. In the numerical integrations, we start from a set of random initial conditions until E_N reaches a steady value.

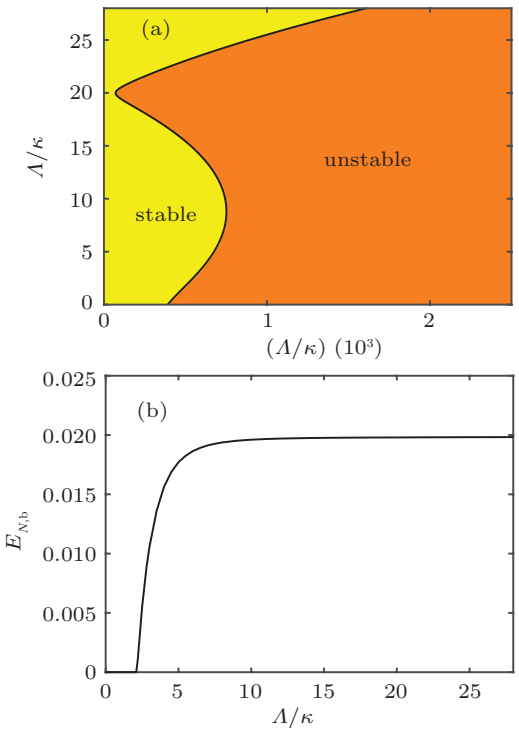


Fig. 1. (a) Two-dimensional stability diagram of the system with respect to the driving amplitude Λ/κ and driving detuning Δ/κ, where parameters used are $g_0/\kappa = 0.02$, $\omega_{\rm m}/\kappa = 20$, and $\gamma_{\rm m}/\kappa = 0.01$. The yellow part on the left is the stable area, and the blue part on the right is the unstable area. This color division is the result of numerical calculation, while the black boundary curve is given by a lengthy analytical expression. (b) The corresponding boundary entanglement $E_{N,\rm b}$ of panel (a) as a function of driving detuning Δ/κ with $\bar{n} = 0$.

Figure 1(b) shows the boundary entanglement $E_{N,\rm b}$ of Fig. 1(a) as a function of driving detuning. The entanglement rapidly increases from zero to a saturation value $\simeq 0.0198$. In the case of resonant driving with $\Delta/\kappa = \omega_{\rm m}/\kappa = 20$, the efficiency of generating entanglement is the highest and the threshold of instability is the lowest. While in the case of driving away from resonance, the instability threshold increases despite the decrease in efficiency. These two factors compensate each other to keep the boundary entanglement increasing more and more slowly as the detuning increases, almost looking like a horizontal line. The entanglement values are all very close to the saturation value 0.0198 for $\Delta/\kappa \in [15, 28]$. This segment can be regarded as having a invariant boundary entanglement value. It cannot be invariant in the entire

range, because different segment ranges may correspond to different interactions. When Δ/κ is close to zero, the effective Hamiltonian has another half contribution from the beam splitter interaction $\propto g_0(a\delta\hat{a}^\dagger\delta\hat{b}+a^*\delta\hat{a}\delta\hat{b}^\dagger)$, and the entanglement is zero. By increasing the driving detuning, the two-mode squeezing term becomes more important and the entanglement increases quickly to a saturation value. This slower and slower increasing behavior of boundary entanglement is also true for Δ/κ goes beyond 28. But when Δ/κ is large to a certain extent, the contribution of both two-mode squeezing and beam-splitter interactions are negligible due to large detuning, the whole system is always stable. Thus the boundary line will first increase and then drop down as the driving amplitude increases. The smaller the mechanical frequency, the smaller the value of Δ/κ at the turning point where the boundary line rises and then falls. We are only interested in the vicinity of the resonant driving where the parametric down conversion is most prominent, so the maximum Δ/κ is set to be 28. In our former work,[11,12] the phenomenon of invariant boundary entanglement has been discovered around the resonant driving, here we give its overall change based on a simpler system, and further find that the boundary entanglement is actually nearly invariant in a larger driving detuning interval.

3. Weak *versus* strong dissipation

In this section, we will first try to figure out how this saturation value of boundary entanglement depends on system parameters. Since this value is also the boundary entanglement at resonant driving $\Delta/\kappa=\omega_{\rm m}/\kappa$, this special boundary point can be focused for analysis. Here, we take advantage of analytical calculation, which cannot be possible in the three-mode system. In the case of $\omega_{\rm m}\gg\gamma_{\rm m}$ and after the rotating wave approximation with $\Delta=\omega_{\rm m}$, the linearized quantum Langevin equation can be equivalently written as follows:[1]

$$\begin{aligned}\delta\dot{\hat{a}}&=\left(\mathrm{i}\omega_{\rm m}-\frac{\kappa}{2}\right)\delta\hat{a}+\frac{\sqrt{2}}{2}\mathrm{i}g_0a\delta\hat{b}^\dagger+\sqrt{\kappa}\hat{a}_{\rm in},\\ \delta\dot{\hat{b}}&=\left(-\mathrm{i}\omega_{\rm m}-\frac{\gamma_{\rm m}}{2}\right)\delta\hat{b}+\frac{\sqrt{2}}{2}\mathrm{i}g_0a\delta\hat{a}^\dagger+\sqrt{\gamma_{\rm m}}\hat{b}_{\rm in},\end{aligned}\quad(6)$$

where $\hat{b}_{\rm in}$ accounting for zero mean input noise for mechanical vibration satisfies $\langle\hat{b}_{\rm in}(t)\hat{b}_{\rm in}^\dagger(t')\rangle=(\bar{n}+1)\delta(t-t')$ and $\langle\hat{b}_{\rm in}^\dagger(t)\hat{b}_{\rm in}(t')\rangle=\bar{n}\delta(t-t')$. By standard Fourier transformation method,[9] we can get the solution for steady-state covariance matrix as

$$V(\infty)=\begin{pmatrix}V_{11}&0&0&V_{14}\\0&V_{11}&V_{14}&0\\0&V_{14}&V_{33}&0\\V_{14}&0&0&V_{33}\end{pmatrix}\quad(7)$$

with

$$\begin{aligned}V_{11}&=\frac{-\gamma_{\rm m}(2g_0^2|a_{\rm s}|^2+\kappa\gamma_{\rm m})}{2(2g_0^2|a_{\rm s}|^2-\kappa\gamma_{\rm m})(\gamma_{\rm m}+\kappa)}+\frac{\kappa}{2(\gamma_{\rm m}+\kappa)},\\ V_{33}&=\frac{-\kappa(2g_0^2|a_{\rm s}|^2+\kappa\gamma_{\rm m})}{2(2g_0^2|a_{\rm s}|^2-\kappa\gamma_{\rm m})(\gamma_{\rm m}+\kappa)}+\frac{\gamma_{\rm m}}{2(\gamma_{\rm m}+\kappa)},\\ V_{14}&=\frac{-\sqrt{2}g_0|a_{\rm s}|\kappa\gamma_{\rm m}}{(2g_0^2|a_{\rm s}|^2-\kappa\gamma_{\rm m})(\gamma_{\rm m}+\kappa)},\end{aligned}\quad(8)$$

where we have set $\bar{n}=0$ for simplicity. All the elements only depend on two ratios: $g_0|a_{\rm s}|/\kappa$ and $\gamma_{\rm m}/\kappa$. After substituting them into the smaller symplectic eigenvalue

$$\eta^-=\frac{1}{2}(V_{11}+V_{33})-\frac{1}{2}\sqrt{(V_{11}-V_{33})^2+4V_{14}^2},$$

the steady-state entanglement at resonant driving $E_{N,\rm res}$ is also a function of $g_0^2|a_{\rm s}|^2/\kappa^2$ and $\gamma_{\rm m}/\kappa$.

The boundary point can be found by demanding the total effective mechanical damping rate $\gamma_{\rm eff}=\gamma_{\rm m}+\gamma_{\rm opt}=0$, where $\gamma_{\rm opt}$ is the optomechanical damping induced by the radiation pressure force.[1] In the resolved sideband regime ($\omega_{\rm m}\gg\kappa$), $\gamma_{\rm opt}\simeq-2g_0^2|a_{\rm s}|^2/\kappa$.[1] Combined with $|a_{\rm s}|^2\simeq\Lambda^2/(\kappa^2/4+\omega_{\rm m}^2)$, we can obtain the resonant driving threshold

$$\Lambda_{\rm th,res}\simeq\frac{\omega_{\rm m}\sqrt{\gamma_{\rm m}\kappa}}{\sqrt{2}g_0},\quad(9)$$

and the corresponding boundary entanglement

$$E_{N,\rm b,res}\simeq-\ln\left(1-\frac{2\gamma_{\rm m}\kappa}{(\kappa+\gamma_{\rm m})^2}\right).\quad(10)$$

It is interesting that $E_{N,\rm b,res}$ is only determined by the ratio $\gamma_{\rm m}/\kappa$. As already mentioned, the steady-state entanglement has two variables, *i.e.*, $E_{N,\rm res}(g_0^2|a_{\rm s}|^2/\kappa^2,\gamma_{\rm m}/\kappa)$. Especially at the boundary, $g_0^2|a_{\rm s}|^2/\kappa^2\simeq g_0^2\Lambda_{\rm th,res}^2/(\omega_{\rm m}^2\kappa^2)\simeq\gamma_{\rm m}/(2\kappa)$, which immediately leads to $E_{N,\rm b,res}(\gamma_{\rm m}/\kappa)$. Furthermore, these two expressions are symmetric with respect to interchanging $\gamma_{\rm m}$ and κ. This is due to the symmetry implicit in Eq. (6) that the status of the two interacting modes is equal, except their damping rates are different. If $\gamma_{\rm m}\ll\kappa$ as assumed above, the vibrational degree of freedom gets instability to produce optomechanical phonon lasing, while in the opposite case $\gamma_{\rm m}\gg\kappa$, the optical cavity mode undergoes transition to optomechanical Brillouin lasing when the effective optical decay rate $\kappa_{\rm eff}$ goes to zero.[29] Because of the inherent symmetry, equations (9) and (10) derived in smaller mechanical damping rate actually work in all ratios of $\gamma_{\rm m}$ and κ as long as $\omega_{\rm m}\gg\gamma_{\rm m}$.

The boundary entanglement at resonant driving $E_{N,\rm b,res}$ as a function of $\gamma_{\rm m}/\kappa$ is plotted in Fig. 2. It increases linearly when $\gamma_{\rm m}/\kappa$ is very small, *i.e.*, $E_{N,\rm b,res}\simeq2\gamma_{\rm m}/\kappa$, further increases with the increase of $\gamma_{\rm m}/\kappa$ to reach a maximum at $\gamma_{\rm m}/\kappa=1$, then decrease monotonously when $\gamma_{\rm m}/\kappa>1$. The numerical integration adopted in Section 2 and the analytical result in Eq. (10) agree very well almost in the whole range, only deviating a little bit when $\gamma_{\rm m}/\omega_{\rm m}$ is larger than 0.1. When $\gamma_{\rm m}$ is very small, the boundary threshold power $\Lambda_{\rm th,res}^2$ is also weak, resulting in small entanglement.

Increasing γ_m can raise the threshold power $\Lambda^2_{th,res}$, thus enlarge the effective coupling strength $g_0 a_s$. However, the larger γ_m, the more impact from the environmental noise. There is a trade-off between these two factors. From the symmetry, the entanglement $E_{N,b,res}$ only depends on ratio of two damping rates and none of the two modes is more special. Consequently $E_{N,b,res}(\gamma_m/\kappa) = E_{N,b,res}(\kappa/\gamma_m)$ and the maximum is achieved when $\gamma_m/\kappa = \kappa/\gamma_m = 1$. There is one by one correspondence for all the other ratios, for example $E_{N,b,res}(0.5) = E_{N,b,res}(2) \simeq 0.588$.

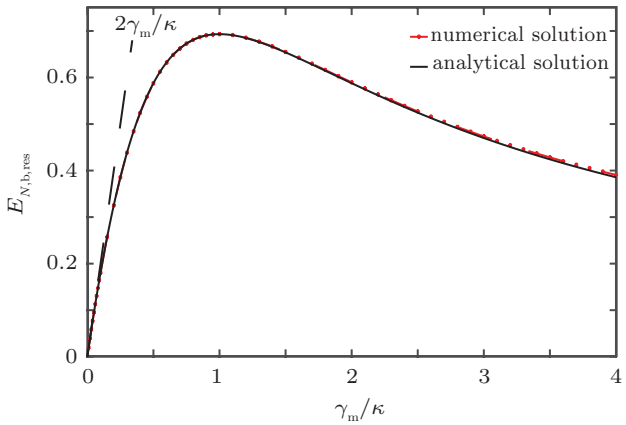


Fig. 2. Variation of boundary entanglement at resonant driving $E_{N,b,res}$ (*i.e.*, boundary entanglement at $\Delta/\kappa = \omega_m/\kappa$) with mechanical damping rate γ_m/κ, where solid black line is plotted by Eq. (10), and the red dotted line is obtained from numerical calculation with the same parameters as in Fig. 1 except that γ_m/κ is now a variable. The curve satisfies a linear relationship $E_{N,b,res} \simeq 2\gamma_m/\kappa$ when γ_m/κ is very small.

To check how the ratio γ_m/κ affect the boundary entanglement, we compare the boundary entanglement with different values of γ_m/κ, while keeping all the other parameters fixed, therefore only the mechanical quality factor Q is varied. Figure 3(a) shows the boundary curves under different choices of γ_m/κ. The resonant driving threshold moves to the right in proportional to $\sqrt{\gamma_m/\kappa}$, and the peak pointing to the left gets more and more sharper until $\gamma_m/\kappa = 1$. The $\gamma_m/\kappa = 0.5$ and 2 correspond to each other in $E_{N,b,res}$ and their boundary lines are almost coincident under the driving of large detuning. The impact of γ_m/κ on the boundary entanglement is significant. The boundary entanglement with weak and strong mechanical damping rates are shown in Figs. 3(b) and 3(c) respectively. The nearly invariant boundary entanglement only appears in the weak dissipation regime. In Fig. 3(a), the saturation value increases linearly with the increase of γ_m/κ, and meanwhile the curves have a more obvious upward trend with increasing driving detuning. In order to achieve a very good invariant entanglement result, *i.e.*, the difference between the maximum and minimum is on the order of one thousandth, the mechanical Q factor should be larger than 10^3. This is well within the linear relationship segment in Fig. 2. In the case of strong dissipation, this phenomenon of nearly invariant boundary entanglement disappears completely. The $\gamma_m/\kappa = 1$ curve is on the top, and curves for $\gamma_m/\kappa = 0.5$ and 2 have two intersections, where one of them is at the resonant driving $\Delta/\kappa = 20$, as seen in Fig. 3(c). In the three-mode system, the value of invariant boundary entanglement with γ_m/κ much smaller than 1 is approximately $(3/2)\gamma_m/\kappa$, with only a different linear coefficient,[12] while the parameter space with large mechanical damping rates has not being touched.

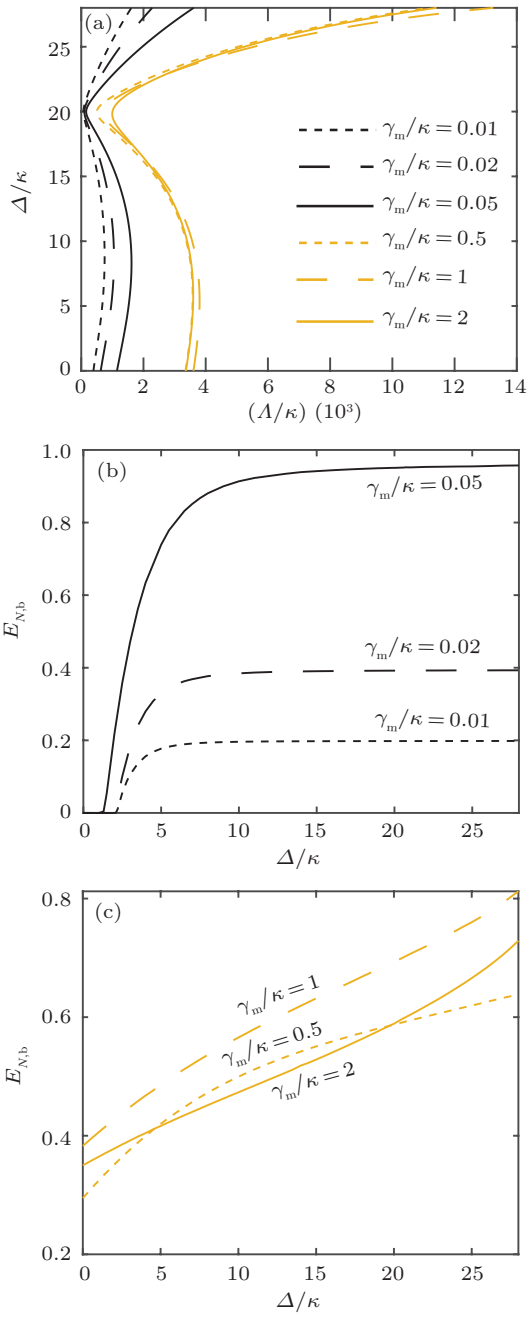


Fig. 3. (a) Stability boundary curves with different mechanical damping rates γ_m/κ, while keeping all the other parameters as in Fig. 1. The corresponding boundary entanglement curves are divided into two groups of weak and strong dissipation, respectively, placed in panels (b) and (c) for comparisons.

4. Discussion on weakly dissipative region

In the following, we will elaborate on how other parameters affect the boundary entanglement in the weak dissipation

regime. The $\gamma_m/\kappa = 0.01$ is fixed as that in Fig. 1 for comparisons, so the remaining parameters are g_0/κ, ω_m/κ, and $\bar{n}$. While discussing one of the them, the other parameters are the same as in Fig. 1.

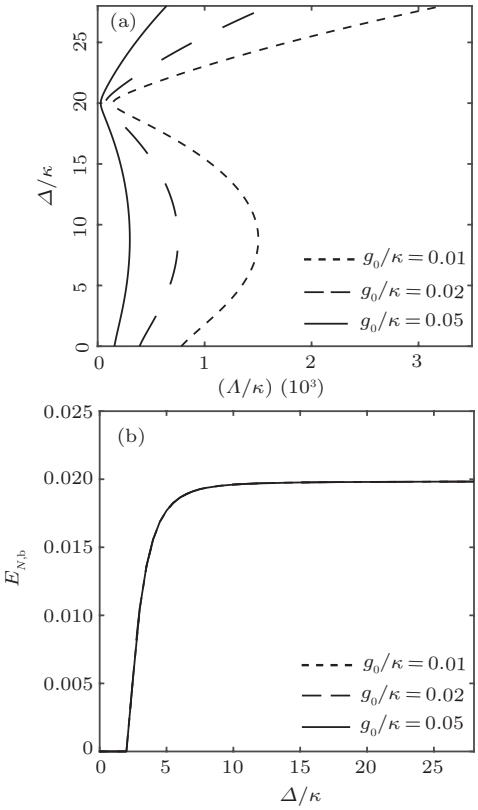


Fig. 4. Stability boundary curves and corresponding boundary entanglement with different choices of g_0/κ are given in panels (a) and (b) respectively, while keeping all the other parameters as those in Fig. 1.

Figure 4(a) depicts the boundary curves for different values of g_0/κ and figure 4(b) shows that the corresponding curves for boundary entanglement completely overlap. As g_0/κ increases, the boundary line moves to the right and becomes sharper. However, the key point is that values of $g_0^2|a_s|^2/\kappa^2$ for different boundary curves are all equal for the same detuning Δ/κ. This can be understood from $\gamma_{opt} \simeq \frac{1}{2}g_0^2|a_s|^2\kappa([\kappa^2/4+(\Delta+\omega_m)^2]^{-1}-[\kappa^2/4+(\Delta-\omega_m)^2]^{-1})$ for $\gamma_m \ll \kappa$,[1] therefore $\gamma_m + \gamma_{opt} = 0$ leads to $g_0^2|a_s|^2/\kappa^2 = F(\gamma_m/\kappa, \Delta/\kappa, \omega_m/\kappa)$. With γ_m/κ and ω_m/κ unchanged, $g_0^2|a_s|^2/\kappa^2$ is only a function of Δ/κ. In the most general case, the boundary entanglement is a function of four variables, *i.e.*, $E_{N,b}(g_0^2|a_s|^2/\kappa^2, \gamma_m/\kappa, \omega_m/\kappa, \Delta/\kappa)$, which combines with the feature just analyzed, can explains straightforwardly why the boundary entanglement does not change with g_0/κ. The boundary entanglement curves also overlap with each other for different values of g_0/κ in the three-mode case.[12]

In Fig. 5(a), the resonant driving peaks of boundary lines shift up or down with the mechanical frequency ω_m/κ, and the lowest driving threshold $\Lambda_{th,res}/\kappa$, which is proportional to ω_m/κ, cause the curves to move left and right. The shape of boundary lines below the resonant driving also becomes less concave with smaller ω_m/κ. Figure 5(b) demonstrates the boundary entanglement with different values of ω_m/κ. The entanglement curves have very similar behavior, rising from zero and approaching the same saturation value quickly, which can be approximately viewed as translation of curves. This is consistent with the result that the saturation value is only determined by γ_m/κ. As mentioned above, the condition to observe invariant boundary entanglement in the three-mode system is $2J = \omega_m$. Changing ω_m/κ alone means deviating from that resonant condition, the boundary entanglement curves will drop down with increasing driving detuning.[12] However, if ω_m/κ and J/κ change at the same time to maintain the resonant condition, different curves will overlap in the form of horizontal straight lines.

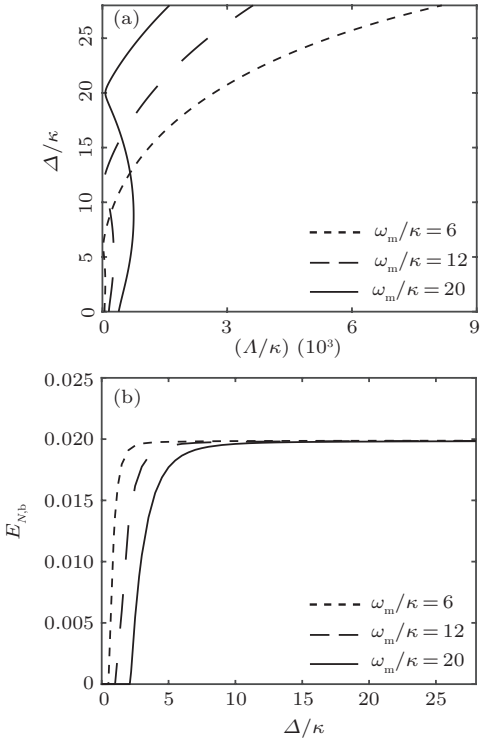


Fig. 5. Stability boundary curves and corresponding boundary entanglement with different choices of ω_m/κ are given in panels (a) and (b) respectively, while keeping all the other parameters as those in Fig. 1.

Finally, the influence from temperature is considered, embodied by the mean thermal phonon number $\bar{n}$. Figure 6(a) shows how the boundary entanglement at resonant driving in Fig. 1(b) varies with $\bar{n}$. It decreases approximately linearly with the increase of $\bar{n}$, *i.e.*, $E_{N,b,res} \simeq \max[0.0198 - 0.0002\bar{n}, 0]$. At $\bar{n} = 100$, the entanglement drops to zero. We expect that the boundary entanglement curve behave similarly as in Fig. 1(b) with only the saturation value decreased with larger $\bar{n}$. However, smaller driving detuning is more sensitive to $\bar{n}$ as shown in Fig. 6(b), thus in contrast to the almost horizontal line with $\bar{n} = 0$, the curves have a more obvious upward trend as $\bar{n}$ increases, reducing the effect of obtaining nearly invariant boundary entanglement in a wide detun-

ing interval. For $\bar{n} = 10$ and $\Delta/\kappa \in [16, 24]$, the difference between the maximum and minimum is about 5%. If you narrow this segment, the difference will be smaller. This is why invariant boundary entanglement can be observed with $\bar{n} = 50$ in our former work.[11] The temperature influence on the boundary entanglement curves has not be discussed in the three-mode case.[12] Figure 6(c) shows the steady-state entanglement $E_{N,\mathrm{res}}$ along the resonant driving $\Delta/\kappa = 20$ with different $\bar{n}$. The entanglement near the instability boundary is robust to thermal phonon noise, while the entanglement far away from the boundary drops down quickly with a non-zero $\bar{n}$. With $\bar{n} = 0$, the entanglement changes very slowly when approaching the boundary, which facilitates the experiment to observe the value of boundary entanglement if the fluctuations of driving field intensity is considered.

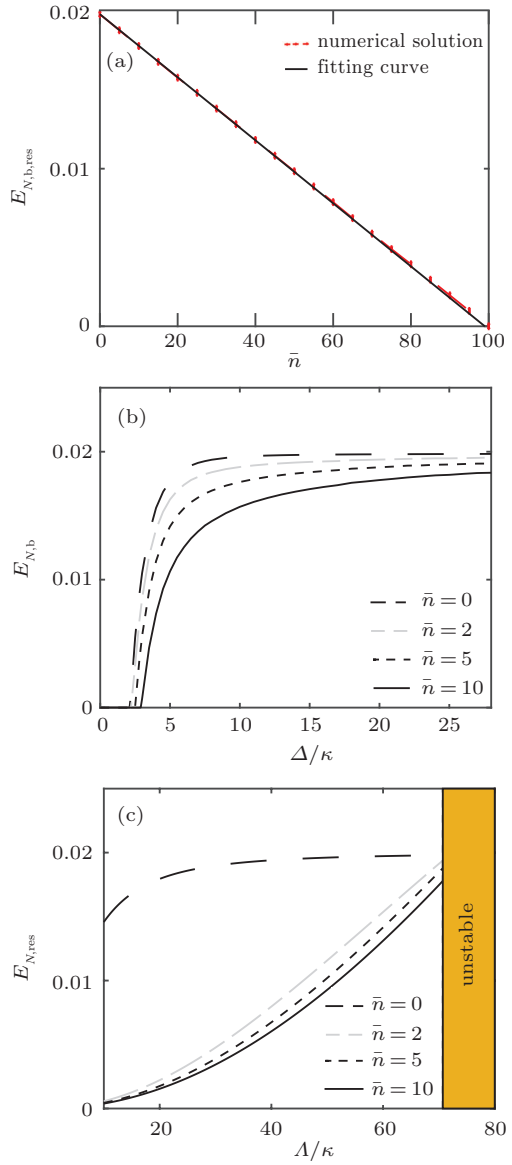


Fig. 6. Influence of temperature on various steady-state entanglement based on the stability diagram in Fig. 1: (a) boundary entanglement at resonant driving $E_{N,\mathrm{b,res}}$ (*i.e.*, $\Delta/\kappa = 20$), where the expression for linear fitting line is given in the main text; (b) the boundary entanglement curve $E_{N,\mathrm{b}}$; (c) the entanglement at resonant driving $E_{N,\mathrm{res}}$, which shows how the entanglement changes when approaching the boundary from the stable region.

5. Conclusion

To summarize, we have studied in detail the boundary entanglement in the simplest two-mode optomechanical system. Through this simpler system, we fully understand the phenomenon of invariant boundary entanglement numerically discovered in our former work.[11,12] The word "invariant" here is by no means completely invariant, but the change in a large parameter range is so small such that we regard it as unchanged. To be more precise, "nearly invariant" boundary entanglement could be better. Besides, all the same parameter dependencies in the weakly dissipative region as that in previous three-mode optomechanical system are obtained, *i.e.*, the value for boundary entanglement is proportional to the ratio of mechanical and optical damping rates, and it does not change with the optomechanical coupling strength or the mechanical frequency.[12] The similarities of both the mechanism in generating the entanglement and the parameter dependence of boundary entanglement fully illustrate that the two-mode system has captured the main characteristics of the three-mode system. Furthermore, we give an overall picture of how the boundary entanglement changes in a much bigger driving detuning interval, assisted by some analytical calculation and combined with the common results of both models to find out that the nearly invariant boundary entanglement is a general phenomenon produced by parametric down conversion in the weakly dissipative region. The temperature will influence the effect of keeping invariant in a wide driving detuning interval. However, with very high mechanical frequency and low temperature, mean thermal phonon number smaller than 1 should be possible. With thermal phonon number almost zero, the value of boundary entanglement could still be observed in spite of fluctuations of driving field intensity. The main challenge is that the invariant boundary entanglement is weak, which might be difficult to measure in realistic system. For example, with $\gamma_{\mathrm{m}}/\kappa \simeq 1.6 \times 10^{-5}$ in Ref. [30], the value for boundary entanglement is only 3.2×10^{-5}. Anyway, the nearly invariant boundary entanglement is definitely interesting as threshold quantum signatures in optomechanical phonon lasers, or might have potential applications where the quantum properties of the boundary is utilized.

Acknowledgment

One of the authors (Zhi-Jiao Deng) is grateful to Jie-Qiao Liao for useful discussions.

References

[1] Aspelmeyer M, Kippenberg T J and Marquardt F 2014 *Rev. Mod. Phys.* **86** 1391
[2] Kippenberg T J and Vahala K J 2007 *Opt. Express* **15** 17172
[3] Peterson G A, Kotler S, Lecocq F, Cicak K, Jin Y, Simmonds R W, Aumentado J and Teufel J D 2019 *Phys. Rev. Lett.* **123** 247701

[4] Liao J Q, Huang J F, Tian L, Kuang L M and Sun C P 2020 *Phys. Rev. A* **101** 063802
[5] Marquardt F and Girvin S M 2009 *Physics* **2** 40
[6] Aspelmeyer M, Meystre P and Schwab K 2012 *Phys. Today* **65** 29
[7] Ludwig M, Kubala B and Marquardt F 2008 *New J. Phys.* **10** 095013
[8] Xu X, Gullans M and Taylor J M 2015 *Phys. Rev. A* **91** 013818
[9] Deng Z J, Habraken S J M and Marquardt F 2016 *New J. Phys.* **18** 063022
[10] Dutta S and Cooper N R 2019 *Phys. Rev. Lett.* **123** 250401
[11] Meng Q X, Deng Z J, Zhu Z and Huang L 2020 *Phys. Rev. A* **101** 023838
[12] Meng Q X, Deng Z J and Cui S W 2020 *Commun. Theor. Phys.* **72** 115101
[13] Law C K 1995 *Phys. Rev. A* **51** 2537
[14] Roque T F, Marquardt F and Yevtushenko O M 2020 *New J. Phys.* **22** 013049
[15] Ghobadi R, Bahrampour A R and Simon C 2011 *Phys. Rev. A* **84** 033846
[16] Vitali D, Gigan S, Ferreira A, Böhm H R, Tombesi P, Guerreiro A, Vedral V, Zeilinger A and Aspelmeyer M 2007 *Phys. Rev. Lett.* **98** 030405
[17] Nejad A A, Askari H R and Baghshahi H R 2017 *Chin. Phys. Lett.* **34** 084205
[18] Benguria R and Kac M 1981 *Phys. Rev. Lett.* **46** 1
[19] Aldana S, Bruder C and Nunnenkamp A 2013 *Phys. Rev. A* **88** 043826
[20] Marquardt F, Harris J G E and Girvin S M 2006 *Phys. Rev. Lett.* **96** 103901
[21] Bakemeier L, Alvermann A and Fehske H 2015 *Phys. Rev. Lett.* **114** 013601
[22] Wang G, Huang L, Lai Y C and Grebogi C 2014 *Phys. Rev. Lett.* **112** 110406
[23] Wang Y D and Clerk A A 2013 *Phys. Rev. Lett.* **110** 253601
[24] Tian L 2013 *Phys. Rev. Lett.* **110** 233602
[25] Yan X B 2017 *Phys. Rev. A* **96** 053831
[26] Yan X B, Deng Z J, Tian Y D and Wu J H 2019 *Opt. Express* **27** 24393
[27] Vidal G and Werner R F 2002 *Phys. Rev. A* **65** 032314
[28] Wu Q, Xiao Y and Zhang Z M 2015 *Chin. Phys. B* **25** 014023
[29] Nunnenkamp A, Sudhir V, Feofanov A K, Roulet A and Kippenberg T J 2014 *Phys. Rev. Lett.* **113** 023604
[30] Hong S, Riedinger R, Marinković I, Wallucks A, Hofer S G, Norte R A, Aspelmeyer M and Grö blacher S 2017 *Science* **358** 203